Simulation of Flow in Stirred Vessel with Axial Flow Impeller: Zonal Modeling and Optimization of Parameters

A. K. Sahu, P. Kumar, and J. B. Joshi*

Department of Chemical Technology, University of Mumbai, Matunga, Mumbai 400 019, India

The usefulness of the turbulent k-ϵ model for simulation of flow in a stirred vessel was studied in detail. For optimization, the effects of model parameters on flow characteristics were analyzed. It was observed that, any single set of model parameters could not yield even reasonable agreement between the model predictions and the experimental observations throughout the vessel. Therefore, the concept of zonal modeling was introduced for the r-z plane. It was observed that with the introduction of zonal modeling, the predicted values of flow variables, except the energy dissipation rate, were in good agreement with experimental data even close to the top surface of the tank. The same results could not be obtained with the standard set of parameters and a single zone. Local turbulent energy dissipation rate (ϵ) was calculated using the expression ($\epsilon = k^{3/2}/L_{res}$) proposed by Wu and Patterson (1989). The zonal modeling prediction was better than the prediction by a standard set of parameters. However, above the impeller, a wide discrepancy between the predicted and experimental value for energy dissipation rate was observed.

Introduction

The development of fast computers has made the design of efficient and robust equipment relatively easier in various branches of engineering. In chemical engineering, reactor design is ubiquitous. In earlier times, the design was based on empirical correlations, working experience, and intuitive knowledge. There have been continuous efforts for the development of rational design procedures. The biggest obstacle has been the understanding of complex fluid mechanics prevailing in the reactors. However, with the emergence of sophisticated measurement techniques, such as laser Doppler anemometry, and the development of various turbulence models to simulate complicated turbulent flows, there has been some progress in the development of reliable design procedures.

The experimental investigation of flow patterns in mechanically agitated tanks with axial flow impellers has been extensively carried out during the last 30 years (Table 1). In the beginning, measurement was confined to mean velocity profiles only. With the advent of modern measurement techniques, it was possible to measure the turbulent flow characteristics along with the mean velocity profiles. However, to obtain flow characteristics in the entire vessel by experiments is not an easy task. Therefore, attempts are being made to predict the turbulent flow profiles in a stirred vessel by developing mathematical models. The accuracy of mathematical modeling of the flow in an agitated tank varies with the degree of sophistication of the model. For the sake of simplicity, various analytical models (Desouza and Pike, 1972; Drbohlav et al., 1978; Platzer and Noll, 1981; Fort, 1986) were devised to predict the mean flow velocities. However, these simplified models did not display the turbulent characteristics of flow patterns. The development of some effective turbulent models, such as k-ϵ and algebraic stress models (ASM), led researchers (Harvey and Greaves, 1982; Placek et al., 1978; Platzer, 1981) to present numerical solutions of the fully developed turbulent flow in a baffled stirred tank. The numerical solution depends on a chosen mathematical model, so different mathematical models have been used to evaluate their efficiency (Bakker and Van den Akker, 1994; Armenante and Chou, 1996). For the sake of brevity, details regarding mathematical models, numerical methods, and grid size, etc. have been summarized in Table 2. In the present paper, it is of interest to highlight the contribution of various research workers and the shortcomings of the various turbulent models. It is also of interest, if possible, to devise some procedures to improve the performance of the turbulent model.

Ranade et al. (1989b) employed the k-ϵ model for simulation of a stirred vessel and observed that the predicted turbulent kinetic energy was overpredicted near the vessel bottom and that the energy dissipation rate was not verified because the experimental data were not available. Based on the suggestions made by Abujelala and Lilly (1984), they reported that, with the variation of parameter values C_2 and C_D, the overall error between the experimental data and the predictions could be minimized. But detailed optimization of the model parameters was not attempted. Bakker and Van den Akker (1994) used ASM and k-ϵ models and observed that the RMS value obtained by the ASM model agrees better with the experimental data than the values predicted by the k-ϵ model. However, above the impeller, the discrepancy between predicted and experimental axial velocity, was large irrespective of the model.

Fokema et al. (1994) analyzed the importance of specifying proper boundary conditions for the prediction of flow characteristics by using two sets of data obtained from two different off-bottom clearances. They modeled the impeller using a thin disk with inlets across both surfaces. For axial velocity, the agreement between the

* Author to whom correspondence should be addressed. E-mail: jbj@udct.ernet.in. Fax: 091-022-4145614.

S0888-5885(97)00321-7 CCC: $15.00
Published on Web 04/14/1998

Table 1. Experimental Details

author	measurement technique	vessel dimension T, mm	impeller type, dimension and location	range of measurement		remarks
				radial	axial	
Fort (1967)	phtoographic method	290	propeller, $D = 72.5$ mm, 96.6 mm; $H_c/T = 0.155, 0.25, 0.333, 0.431$			measurement made only close to the impeller
Fort et al. (1971)	pilot tube	290	paddle, $D = 96.66$ mm, 72.5 mm, 58 mm; $H_c/T = 1/4$	up to the wall	just below and above the impeller	
Tatterson et al. (1980)	stereoscopic visualization	295, 914	PTD, $D = 102$ mm, 305 mm; $H_c/T = 1/3$			only the general nature of flow was observed
Ranade and Joshi (1989a)	LDA	300, 500	PTD, $D = 75$ mm, 100 mm, 150 mm, 167 mm; $H_c/T = 1/3, 1/4, 1/6$	up to $r = 0.95$	up to 20 mm above the bottom and above the impeller up to $z = 0.74$	
Fort et al. (1991)	LDA	297	PTD, $D = 99$ mm; $H_c/T = 1/3$	up to the wall	just below and above the impeller blade	
Jaworski et al. (1991)	LDA	146	PTD, $D = 48.67$ mm; $H_c/T = 1/2, 1/4$	up to $r = 0.96$	up to 6 mm above the bottom and up to 56.5 mm above the impeller	
Ranade et al. (1991)	LDA	300, 500	PTD, $D = 75$ mm, 100 mm, 150 mm, 167 mm; $H_c/T = 1/3, 1/4, 1/6$	up to $r = 0.95$	up to 20 mm above the bottom and $z = 0.66$ above the impeller	data from Ranade and Joshi (1989)
Ranade et al. (1992)	LDA	500	PTD with blade angles 30, 45, 60 deg, and five other designs of axial flow impellers; $D = 167$ mm; $H_c/T = 1/2$	up to $r = 0.95$	up to $z = 0.37$ below the impeller and up to $z = 0.2$ above the impeller	
Kresta and Wood (1993a)	LDA	152.4	PTD, $D = 76.2$ mm, 50.8 mm; H_c/T varied from 1/2 to 1/20	up to $r = 1$	up to 40.4 mm below the impeller	
Kresta and Wood (1993b)	LDA	152.4	PTD, $D = 76.2$ mm; $H_c/T = 1/4$	up to $r = 0.58$	at 2 mm below the lower edge of the impeller blade	
Bakker and Van den Akker (1994)	LDA	444	PTD, A315, $D = 177.6$ mm; $H_c/T = 0.3$			
Fokema et al. (1994)	LDA	150	PTD, $D = 75$ mm; $H_c/T = 0.465, 0.25$	up to $r = 1$	up to 32.3 mm below the impeller	
Sahu and Joshi (1995)	LDA	500	PTD1, PTD2, CURPTD, MODPTD, PROP, MPTD, $D = 167$ mm, 155 mm (PTD2); $H_c/T = 1/2$	up to $r = 0.95$	up to $z = 0.52$ below the impeller and up to $z = 0.56$ above the impeller	data from Ranade et al. (1992)
Armenante and Chou (1996)	LDA	290	PTD, $D = 102$ mm; $H_c/T = 0.414$	up to $r = 0.85$	above up to 169 mm, and below up to 82.8 mm	
Harris et al. (1996)	LDA	300	PTD, $D = 75$ mm, 100 mm, 150 mm, 167 mm; $H_c/T = 1/3, 1/4, 1/6$	up to $r = 0.95$	up to 20 mm above the bottom and up to $z = 0.366$ above the impeller	data from Ranade and Joshi (1989)
Hockey and Nouri (1996)	LDA	294	PTD, $D = 98$ mm; $H_c/T = 1/3$	up to $r = 0.83$		
Ranade and Dommeti (1996)	LDA	300	PTD, $D = 100$ mm; $H_c/T = 1/3$	up to $r = 0.95$	up to 20 mm above the bottom and up to $z = 0.366$ above the impeller	data from Ranade and Joshi (1989)
Xu and Mcgrath (1996)	LDA	305	PTD, $D = 101.67$ mm; $H_c/T = 1/3$	up to $r = 0.5$	above the impeller up to 3 mm and below up to 49 mm	

Table 2. Numerical Details

author	model	algorithm	CFD code	scheme	grid size (r, θ, z)	range of prediction		CMV made	CTP made	P_p/P_e
						radial	axial			
Pericleous and Patel (1987)		SIMPLEST	PHOENICS			up to $r = 0.2$	up to 50 mm above the impeller and 50 mm below the impeller	u, v		
Ranade and Joshi (1989b)	k-ϵ	SIMPLER	in-house	power-law	$30 \times 5 \times 46$	up to $r = 0.96$	up to $z = 0.366$ above the impeller and up to $z = 0.533$ below the impeller	u, v, w	k	0.9
Ranade et al. (1991)	k-ϵ	SIMPLER	in-house	power-law	$15 \times 16 \times 31$	up to $r = 0.96$	up to $z = 0.366$ above the impeller and up to $z = 0.533$ below the impeller	u, v, w	k	0.9
Ranade et al. (1992)	k-ϵ	SIMPLER	in-house	power-law	$30 \times 5 \times 46$	up to $r = 0.95$	up to $z = 0.2$ above the impeller and up to $z = 0.37$ below the impeller	u, v, w	k	
Bakker and Van den Akker (1994)	k-ϵ and ASM		FLUENT	power-law	$25 \times 25 \times 40$			v	u	
Fokema et al (1994)	k-ϵ	SIMPLEC	FLOW3D	hybrid	$20 \times 20 \times 43$ (nonuniform)	up to $r = 1$	up to 32.34 mm below the impeller	v	k,ϵ	
Sahu and Joshi (1995)	k-ϵ	SIMPLE	in-house	power-law, hybrid, upwind	28×33 (r, z)	up to $r = 0.96$	up to $z = 0.56$ above the impeller and up to $z = 0.52$ below the impeller	u, v	k	1.6
Armenante and Chou (1996)	k-ϵ and ASM		FLUENT		(24, 696) node points	up to $r = 0.95$	up to 169.2 mm above the impeller and up to 82.8 mm below the impeller	u, v, w	k,ϵ	0.11
Harris et al. (1996)	k-ϵ and Reynolds stress		FLOW3D		$60 \times 16 \times 58$	up to $r = 0.95$	up to $z = 0.366$ above the impeller and up to $z = 0.533$ below the impeller	u	k	
Ranade and Dommeti (1996)	k-ϵ		FLUENT		$35 \times 38 \times 46$	up to $r = 0.95$	up to $z = 0.366$ above the impeller and up to $z = 0.533$ below the impeller	u, v, w		0.8
Xu and Mcgrath (1996)	Reynolds stress		FLOW3D			up to $r = 0.5$	up to 3 mm above the impeller and up to 49 mm below the impeller	u, v, w		1.1

predicted and the experimental values was excellent. However, the comparison was presented for a region close to the impeller and no comparison was made near the wall. The predicted energy dissipation rate profiles immediately below the impeller were of the correct magnitude and attained peak values just beyond the tip of the impeller. However, as one moves away from the impeller, the predicted values of ϵ decayed to only a fraction of the experimental values. It was also observed that the ratio of average dissipation rate in the impeller region to the average dissipation rate in the tank was 5.3 for the high clearance case and 5.9 for the low clearance case. These findings were in good agreement with those experimentally determined by Jaworski and Fort (1991).

Sahu and Joshi (1995) reviewed the literature and pointed out the need to study the effect of various numerical schemes, initial guess values of the flow variables, underrelaxation parameters, internal iterations, etc., on the rate of convergence and the effect of model parameters on the flow variables. Further, they investigated the effect of the global grid size and near wall grid size on the solution. They studied six designs of axial flow impeller and observed that there was a qualitative agreement between the predicted and experimental results in the impeller region. However, away from the impeller, particularly in the upper part of the vessel, differences were large between predicted and experimental values.

In a recent study, Armenante and Chou (1996) opined that the use of an isotropic turbulence model and specification of experimental data only on the bottom surface of the impeller-swept volume were probably the limitations of previous CFD analysis. They provided measured values of flow characteristics below and above the impeller-swept volume and also used ASM and k-ϵ models. In the upper part of the vessel, a wide difference between the experimental and predicted values was found for both the models. However, the difference between the values predicted by ASM and k-ϵ was very small. Harris et al. (1996) reviewed the recent progress in the predictions of flow in baffled stirred tank reactors. They found that the comparison between three-dimensional (3D) simulation predictions and the experimental results reported in the literature generally exhibited good agreement for radial and axial components of mean velocity, whereas the tangential velocity component was less well predicted, with anisotropic models yielding superior results. One area of major concern has been the prediction of turbulent quantities, especially ϵ. Some of the works in the literature yielded good results in the impeller stream, but elsewhere in the vessel, predictions were generally poor. Simulations carried out both by the inner-outer method (Brucato et al., 1994) and by providing impeller boundary conditions can be found in the literature. In the simulation using boundary conditions, mean radial velocities were in good agreement with the experimental results. The most important observation was that both the models yielded similar predictions. In both the models, the turbulent kinetic energy and its dissipation rate were underpredicted in the impeller stream. It was interesting to note that the inner zone simulation yielded values of k in much closer agreement with the experimental data below the impeller than the simulation using impeller boundary conditions. The predicted mean tangential velocity was also in good agreement with the experimental observations.

Ranade and Dommeti (1996) employed a snapshot method that does not require experimentally measured boundary conditions and could provide solution within the impeller blades. In the case of axial velocity, comparison between the prediction and the experimental data was quite adequate, except for the disagreement near the symmetry axis. For radial and tangential velocities, predictions at locations away from the impeller were also closer to the experimental data. Close to the impeller, both the radial and the tangential velocities were overpredicted. Away from the impeller, the predicted tangential velocity showed a counter-rotating region near the symmetry axis that was not observed in the experimental findings. Xu and Mcgrath (1996) used the momentum source and sink technique to evaluate the impeller boundary conditions. The predicted values were very good for the axial and radial velocities, whereas the tangential velocity was overpredicted. However, the results were presented in the region very close to the impeller. Therefore, the reliability of the method for regions away from the impeller could not be ascertained.

From the discussion of the literature just presented, it is clear that the comparison between the experimental findings and the numerical predictions was generally inadequate, except in regions close to the impeller, irrespective of the mathematical model and the numerical method used for simulation of the impeller boundary conditions. It is well known that for numerical simulation of flow in a stirred tank the turbulence parameter values are the same as that of pipe flow. Rodi (1993) remarked that the turbulent flow parameters (C_1, C_2, C_D) for the k-ϵ model based on pipe flow could not be considered universal and modified these parameters for an axisymmetric jet flow that yielded good agreement with the experimental observations. In stirred vessels, the flow pattern is entirely different from that of pipe flow, so the turbulence parameter values may need modification in conjunction with experimental data to yield a better prediction. Therefore, optimization of parameters related to stirred tanks is desirable. However, from our experience, a single set of parameters did not give good prediction in the entire vessel. Therefore, it was concluded that the disagreement may be the shortcoming of the turbulence model. Although a universal turbulence model is a distant dream, it was shown by Ferziger et al. (1988) that a turbulence model could be made universal with the introduction of zonal modeling. The philosophy of zonal modeling is as follows: With the knowledge of flow pattern, the flow domain is divided into various subdomains. Each subdomain may be called as a zone. In each subdomain, a set of model parameters is chosen and, at the interface, care is taken to maintain the continuity. In the present analysis, the flow domain of our interest was divided into several subdomains and an optimal set of model parameter values were selected by comparing the predicted values with the experimental data. The relative merits of zonal modeling have been brought out clearly.

Mathematical Formulation

A 3D steady flow generated by an axial flow impeller in a cylindrical vessel with four equally spaced baffles was considered. Flow was assumed to be periodic

Table 3. Source Terms for the Generalized Equation

ϕ	Γ_{eff}	S_ϕ
1	0	0
u	$\mu + \mu_t$	$C_D\left[\frac{1}{r}\frac{\partial}{\partial r}\left(r\Gamma_{eff}\frac{\partial u}{\partial r}\right) + \frac{\partial}{\partial z}\left(\Gamma_{eff}\frac{\partial v}{\partial r}\right) + \frac{1}{r}\frac{\partial}{\partial \theta}\left(\Gamma_{eff}\frac{\partial w}{\partial r}\right) - \frac{1}{r}\frac{\partial}{\partial \theta}\left(\Gamma_{eff}\frac{w}{r}\right) - \frac{2\Gamma_{eff}}{r^2}\frac{\partial w}{\partial \theta} - \frac{2\Gamma_{eff}u}{r^2}\right] - \frac{\partial p}{\partial r} - \frac{2}{3}\frac{\partial k}{\partial r} + \frac{w^2}{r}$
v	$\mu + \mu_t$	$C_D\left[\frac{1}{r}\frac{\partial}{\partial r}\left(\Gamma_{eff}\frac{\partial u}{\partial z}\right) + \frac{1}{r}\frac{\partial}{\partial \theta}\left(\Gamma_{eff}\frac{\partial w}{\partial z}\right) + \frac{\partial}{\partial z}\left(\Gamma_{eff}\frac{\partial v}{\partial z}\right)\right] - \frac{2}{3}\frac{\partial k}{\partial z} - \frac{\partial p}{\partial z}$
w	$\mu + \mu_t$	$C_D\left[\frac{1}{r}\frac{\partial}{\partial r}\left(\Gamma_{eff}\frac{\partial u}{\partial \theta}\right) + \frac{\partial}{\partial z}\left(\frac{\Gamma_{eff}}{r}\frac{\partial v}{\partial \theta}\right) + \frac{1}{r}\frac{\partial}{\partial \theta}\left(\frac{\Gamma_{eff}}{r}\frac{\partial w}{\partial \theta}\right) + \Gamma_{eff}\frac{\partial}{\partial r}\left(\frac{w}{r}\right) - \frac{1}{r}\frac{\partial}{\partial r}(\Gamma_{eff}w) + \frac{\Gamma_{eff}}{r^2}\frac{\partial u}{\partial \theta} + \frac{1}{r}\frac{\partial}{\partial \theta}\left(\frac{2\Gamma_{eff}u}{r}\right)\right] - \frac{2}{3}\frac{1}{r}\frac{\partial k}{\partial \theta} - \frac{1}{r}\frac{\partial p}{\partial \theta} - \frac{uw}{r}$
k	$\mu + \mu_t/\sigma_k$	$G - \epsilon$
ϵ	$\mu + \mu_t/\sigma_\epsilon$	$\frac{\epsilon}{k}(C_1G - C_2\epsilon)$
where		$G = C_D\mu_t\left[2\left[\left(\frac{\partial u}{\partial r}\right)^2 + \left(\frac{1}{r}\frac{\partial w}{\partial \theta} + \frac{u}{r}\right)^2 + \left(\frac{\partial v}{\partial z}\right)^2\right] + \left(r\frac{\partial}{\partial r}\left(\frac{w}{r}\right) + \frac{1}{r}\frac{\partial u}{\partial \theta}\right)^2 + \left(\frac{1}{r}\frac{\partial v}{\partial \theta} + \frac{\partial w}{\partial z}\right)^2 + \left(\frac{\partial u}{\partial z} + \frac{\partial v}{\partial r}\right)^2\right]$
		$\mu = \frac{\bar{\mu}}{C_D\rho U_{tip}}$
		$\mu_t = \frac{k^2}{\epsilon}$

because of the presence of baffles at an equal space interval. Hence, a quadrant of the vessel was used for numerical simulation. The standard k-ϵ turbulent model was chosen for numerical simulation. The impeller was placed at H/3 from the vessel bottom. A cylindrical coordinate system was used, with origin located at the impeller center and the angular position $\theta = 0$ coincided with one of the baffle plane. For the sake of sign convention, the 'z' coordinate below the impeller was taken as positive and that above the impeller was negative. The transport equations for a generalized variable ϕ for an incompressible flow in nondimensional coordinate system is written as follows:

$$\frac{1}{r}\frac{\partial}{\partial r}(ur\phi) + \frac{1}{r}\frac{\partial}{\partial \theta}(w\phi) + \frac{\partial}{\partial z}(v\phi) = \frac{1}{r}\frac{\partial}{\partial r}\left(r\Gamma_{eff}\frac{\partial \phi}{\partial r}\right) + \frac{1}{r}\frac{\partial}{\partial \theta}\left(\frac{\Gamma_{eff}}{r}\frac{\partial \phi}{\partial \theta}\right) + \frac{\partial}{\partial z}\left(\Gamma_{eff}\frac{\partial \phi}{\partial z}\right) + S_\phi \quad (1)$$

The expression for Γ_{eff} and S_ϕ are given in Table 3 . The nondimensional procedure is the same as in Sahu and Joshi (1995). The set of boundary condition for eq 1 is as follows:

At $r = 0$ for $z \geq 0$ and all θ,

$$u = \frac{\partial v}{\partial r} = w = \frac{\partial k}{\partial r} = \frac{\partial \epsilon}{\partial r} = 0.0 \quad (2)$$

For $z < 0$, $r = r_s$, for all θ, $u = v = k = \epsilon = 0$; $w = w_s$. At $r = 1$ for all z and θ, $u = v = w = k = \epsilon = 0.0$. At $z = 2/3$ for all r and θ, $u = v = w = k = \epsilon = 0.0$. At $z = -4/3$ for all r and θ,

$$\frac{\partial u}{\partial z} = v = \frac{\partial w}{\partial z} = \frac{\partial k}{\partial z} = \frac{\partial \epsilon}{\partial z} = 0.0 \quad (3)$$

At $\theta = 0$ for all $r > r_b$ and z; $\theta = \pi/2$ for all $r > r_b$ and z, $u = v = w = k = \epsilon = 0.0$.

Numerical Method

For discretizing eq 1, a stable numerical procedure must be used. Recently, Sahu and Joshi (1995) observed that for the simulation of a cylindrical baffled stirred tank, the Power-law scheme was superior to hybrid as well as upwind schemes. After discretization and linearization (same as in Sahu and Joshi, 1995), the set of algebraic equations for each variable was solved iteratively by the line-by-line method (Alternate Direct Implicit Method). An accelerating procedure proposed by Van Doormal and Raithby (1984) to enhance the convergence of the algebraic equations was used. Other details pertaining to numerical procedures are the same as those of Sahu and Joshi (1995), except the solution of the pressure equation. In the present analysis, the rate of convergence of the SIMPLE algorithm (Patankar, 1980) was very slow with an increase in the number of grids. Therefore, the SIMPLER algorithm was employed to solve pressure and mean velocity equations iteratively. Although several methods are available to take into account the no-slip condition (Patel et al.,

1984), in the present analysis, the no-slip condition was replaced by introducing the wall function (Hwang et al., 1993; Launder and Spalding, 1974). Different methods are available for modeling the impeller (Harris et al., 1996); in the present study, measured values of radial, axial and tangential velocities along with turbulent kinetic energy have been provided around the impeller. The energy dissipation was calculated by the iterative method (Sahu and Joshi, 1995). A numerically obtained solution must be grid independent. In the literature, different authors have studied the effects of grid size and recommended different types of grid combinations (Fokema et al., 1994; Bakker and Van den Akker, 1994). In the present study, a grid size of $37 \times 15 \times 40$ (r, θ, z) yielded a grid-independent solution. Computation was carried out with a Pentium-PC. The iterative process was terminated when the mass source residue over each control volume was $<10^{-4}$ and the residual for momentum, turbulent kinetic energy, and turbulent energy dissipation rate was $<10^{-5}$.

Results and Discussion

As mentioned in the *Introduction*, the prime interest of this study was to analyze the usefulness of the k-ϵ model for the simulation of a stirred vessel by optimizing the model parameters and by zonal modeling. However, at the beginning, a brief discussion will be presented regarding the effects of various numerical parameters on the convergence of flow variables and a comparative study between the present analysis and the existing literature.

Effects of Under-relaxation, Initial Guess Values, and Internal Iterations. The under-relaxation parameters for flow variables should be adjusted very carefully to obtain a converged solution. With the increase of grid size, a careful selection of under-relaxation parameters was needed for the calculation of axial and tangential velocities. To begin with the iterative process, the values of the under-relaxation parameters for axial and tangential components were 0.05 and 0.12, respectively. If these under-relaxation parameters were retained during computation, then the iterative process became very slow. To overcome this difficulty, the magnitude of the initial set of under-relaxation parameters were increased in a regular interval depending on the magnitude of the source term or the total number of iterations needed, until the set of parameters attained an optimal value for which convergence was obtained with optimum CPU time. It was observed that these optimal values of under-relaxation parameters were 0.45, 0.35, 0.45, 0.25, and 0.30 for radial, axial, and tangential velocities, turbulent kinetic energy, and turbulent energy dissipation rate, respectively. For the pressure equation, a fixed relaxation parameter of 0.75 was used. For a two-dimensional (2D) flow, Sahu and Joshi (1995) observed that the relation between the relaxation parameters of velocities and pressure correction may be expressed by a simple equation $\alpha_v = 1 - \alpha_p$. A similar observation was made by Peric et al. (1987). However, for a 3D simulation, no such relation could be established. In the case of a 2D flow, the relaxation parameters for axial and radial velocities were the same, whereas for the 3D flow, they were different for different velocity components. In the 2D analysis, initial guess values of k and ϵ had a great influence on the success of the iterative process. Similar observations were also made for the 3D analysis. The internal iterations required for the solution of algebraic equations for different variables are different. For velocities, six internal iterations were sufficient to obtain a converged solution. However, for the turbulent kinetic energy, a minimum of 15−20 internal iterations were required and ∼10 internal iterations were needed for the turbulent energy dissipation rate equation. Although a fixed number of internal iterations was used for the aforementioned variables, for pressure and pressure correction equations, a different procedure was adopted to ensure convergence. To begin with, the internal iterations for pressure and pressure correction equations were taken as two and four, respectively. As the iterative process progressed, these numbers were increased to 15 to expedite the convergence. Normally, the first increment in the number of internal iteration was given after 50 iterations. Later, after an interval of 10 iterations, the internal iterations for pressure and pressure correction equations were incremented.

Comparison between 2D and 3D Predictions. In literature, for the sake of simplicity, various authors (Harvey and Greaves, 1982; Sahu and Joshi, 1995) used the 2D k-ϵ turbulent model to simulate the stirred baffled vessel. Therefore, it was pertinent to give a detailed comparison between experimental data and predicted values that were obtained by employing 2D and 3D models for evaluating the efficiency of the said models. The predicted 3D radial velocity profile at $z = 0.586$ agreed well with the experimental data in the range $r \leq 0.6$, except close to the axis (Figure 1a). The predicted 2D values were higher in this region. Beyond this region the predicted values obtained by both the models were almost the same and close to the experimental values (Figure 1a). At $z = 0.36$ (Figure 1b) and $z = 0.24$ (Figure 1c), the 3D predictions agreed well with the experimental data, whereas 2D solution agreement was good only when $r > 0.4$. Above the impeller, the 2D predictions of radial velocity were better than the 3D prediction ($z = -0.12, -0.96$), except at $z = -0.48$ (Figures 1d, e, and f). The 2D and 3D predicted axial velocity profiles below the impeller were almost the same for $r \geq 0.375$, and their comparison with experimental data was also very good (Figures 2a, b, and c). In contrast, for $r < 0.375$, the 3D predicted solution was very good. As one moved towards the bottom of the vessel from the impeller, the difference between the 2D prediction and experimental data widened near the axis (Figures 2a, b, and c). This disagreement might be due to the omission of the tangential velocity component in the 2D prediction. Above the impeller ($z = -0.12, -0.48, -0.96$), the 3D prediction was in better agreement with experimental data than the 2D prediction (Figures 2d, e, and f). An important behavior of the flow phenomena above the impeller was that the experimentally observed secondary circulation (Figure 2f) was accurately predicted by the 3D model. However, the 2D model failed to demonstrate this behavior, even close to the tank surface. This observation clearly showed the shortcoming of the 2D prediction. The turbulent kinetic energy values predicted by 2D and 3D models were in very good agreement with experimental data at $z = 0.24$ for $r > 0.4$ (Figure 3c). As one moved towards the bottom of the vessel, the 3D model yielded a better agreement with the experimental data than the 2D model (Figures 3a, b, and c). Near the axis, the value

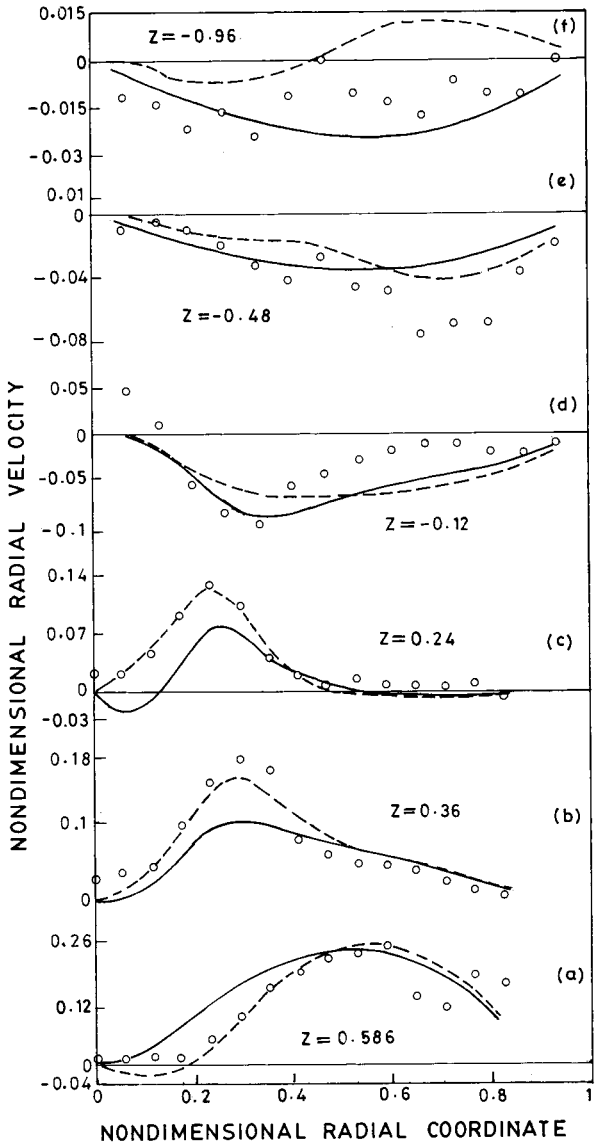

Figure 1. Comparison of 2D and 3D predicted values of radial velocity with experimental value. Key: (—) 2D prediction; (---) 3D prediction; (°°°°°) experimental data.

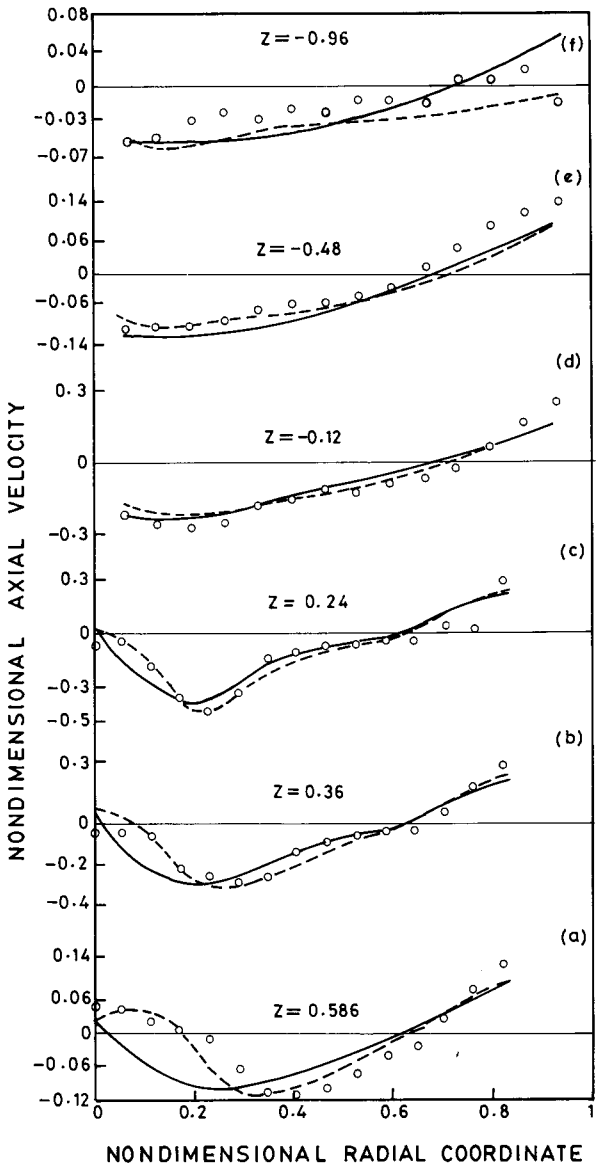

Figure 2. Comparison of 2D and 3D predicted values of axial velocity with experimental value. Symbols are the same as in Figure 1.

of k predicted by the 2D model was much higher than the experimental data (Figures 3a, b, c), unlike the three-dimensional prediction. Above the impeller ($z = -0.12, -0.48, -0.96$), the experimental data for turbulent kinetic energy were very distant from the 2D as well as the 3D predictions (Figures 3d, e, and f). However, as seen in Figures 3e and f, the distribution of the turbulent kinetic energy was more even in the case of the 3D prediction. It was also noticed that below the impeller, the rate of reduction in the value of the turbulent kinetic energy within the region $r < 0.4$ for the 2D model was slower than that of 3D model (Figures 3a, b, and c). This variation further signified the shortcoming of the 2D model. All these observations indicated that the 2D model predictions were not good enough to give the details of the flow phenomena. Therefore, for a better simulation, a 3D model is desirable.

Effect of Model Parameters. Although Sahu and Joshi (1995) discussed in detail the effects of model parameters on the flow characteristics, in the present study a further elaboration was needed in view of the 3D analysis and zonal modeling. Further, the success of the zonal modeling totally depended on the selection of model parameter values in different zones. This selection was possible only by knowing the variation of the flow characteristics in the entire vessel with respect to the turbulent model parameters. The turbulent model parameters σ_k, σ_ϵ, and γ did not influence the flow characteristics to any great extent (Sahu and Joshi, 1995). Therefore, the effect of the remaining three turbulent model parameters C_1, C_2, and C_D was analyzed in detail. With a decrease in value of C_2, the predicted circulation below the impeller and near the axis was increased (Figures 4a and 5a). The maxima of radial, axial, and tangential velocity profiles (Figures 4a and b, 5a and b, and 6a and b) also increased. The tangential velocity at $z = 0.586$ (Figure 6a) near the axis shot up with a decrease in value of C_2. The rapid increase of the profiles was due to the low prediction of the turbulent kinetic energy in that region (Figure 7a). Furthermore, larger circulating zone was observed when the predicted turbulent kinetic energy was small (Figures 5a and 4a). It was interesting to note that below the impeller the predicted turbulent kinetic energy was

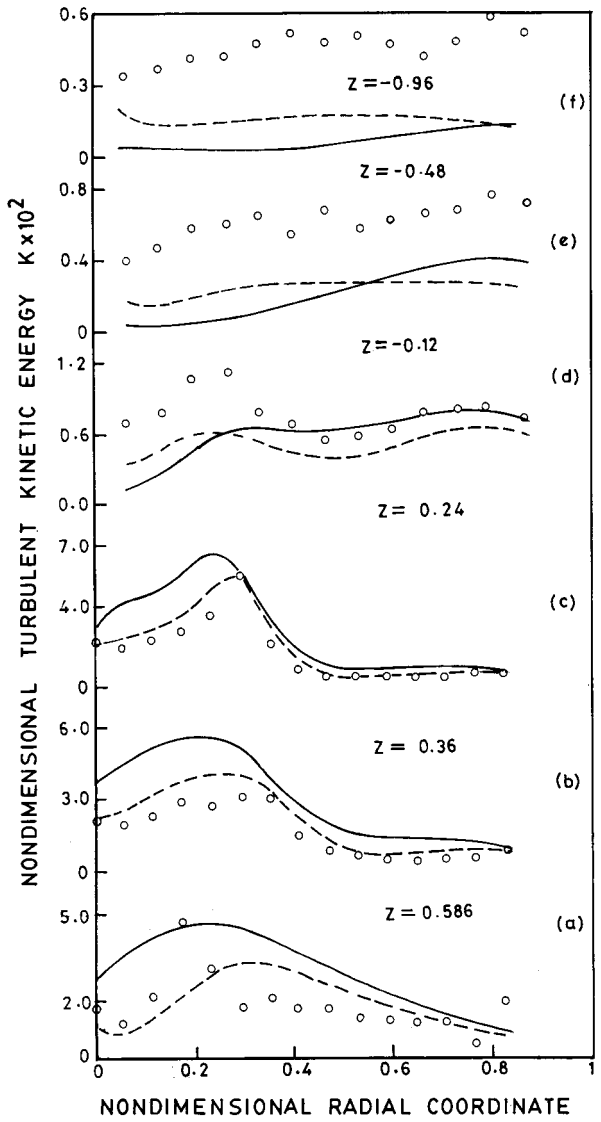

Figure 3. Comparison of 2D and 3D predicted values of turbulent kinetic energy with experimental value. Symbols are the same as in Figure 1.

very sensitive to the parameter C_2 as compared with the other two parameters C_1 and C_D (Figure 7a). However, above the impeller, all the flow characteristics changed with the decrease in the value of C_2 (i.e., predicted turbulent kinetic energy was very low and axial, radial, and tangential velocities were very high). It was also interesting to note that the predicted turbulent kinetic energy below the impeller was closer to the experimental data when the C_2 value was reduced (Figure 7a). The velocity profiles did not vary much with respect to the parameter C_2 (Figures 4a and b, 5a and b, and 6a) below the impeller. All these observations were useful for the purpose of zonal modeling, and the value of C_2 could be conveniently adjusted to get a better agreement with the experimental data below as well as above the impeller. Sahu and Joshi (1995) reported that the parameter C_1 affected the flow characteristics exactly in the opposite way to that of C_2. Similar behavior was also observed in the present study (Figures 4−7). However, an important point to remember is that C_2 affected flow characteristics more vigorously than C_1 (Figures 4−7), particularly in the upper part of the vessel, for the same reduction (15%) from their standard value.

A reduction in the value of C_D yielded a better agreement of the flow characteristics with experimental data at $z = 0.24$ (Figures 4b, 5b, 6b, and 7b). As the value of z was increased, the predicted values of the flow characteristics were overpredicted (Figures 4a and 6a), except the axial velocity (Figure 5a). The predicted turbulent kinetic energy was also higher than the experimental data, although its value was less in comparison with the predicted values that were obtained by a standard set of parameters (Figure 7a). This behavior indicated that, for zonal modeling, the parameter C_D could be conveniently chosen to obtain a better agreement with the experimental data. A similar observation was also made above the impeller. At $z = -0.24$, a better agreement between the predicted velocity profiles and the experimental data was observed for a reduced value of C_D (Figures 4c, 5c, and 6c), whereas the predicted turbulent kinetic energy was lower than the experimental data (Figure 7c). However, with an increase in z in the upward direction, the predicted flow characteristics were higher in magnitude than the experimental data (Figures 4d, 5d, and 6d), except the value of turbulent kinetic energy (Figure 6d). As seen in Figures 4d, 5d, and 6d, although the velocities were overpredicted at $z = -0.96$, the predicted turbulent kinetic energy (Figure 7d) was very low at this position irrespective of the variation of the values of the parameters. However, it is clear that with a decrease in the value of C_D, the magnitude of k increased (Figure 7d). Hence, the parameter C_D could be used along with other parameters for zonal modeling, which might yield a better prediction.

Abujelala and Lilley (1984) reviewed the previous attempts of the modification of standard model parameters with special emphasis on the needs of recirculating flows. They recommended a new set of model constants optimized for the recirculating flow in combustor geometry (i.e., $C_D = 0.125$, $C_1 = 1.44$, $C_2 = 1.6$, $\sigma_\epsilon = 1.3$, $\sigma_k = 1$, and $\gamma = 0.41$). Although this set of new parameters predicted the velocity and the turbulent quantities well below the impeller, above the impeller, the predicted turbulent quantities were far away from the experimental data. Further, from the discussion just presented on the effects of parameters on the flow characteristics, it became very clear that any single set of parameters did not produce good agreement between the experimental data and the predicted values. Furthermore, the observed parametric sensitivity revealed the possibility of getting good agreement between the experimental and the predicted values by using zonal modeling.

Zonal Modeling. To start with, the entire flow domain was divided into two regions horizontally at the impeller center plane and two sets of parameters were selected for each region. The variation of the flow characteristics in one region did not significantly affect the flow characteristics in the other. This observation made it clear that by dividing the flow domain into several zones a better agreement between the experimental and the predicted values could be obtained. Therefore, it was decided to divide the r-z flow domain into several subdomains. The parameter values were selected for each subdomain by trail and error. Each subdomain may be called as a zone. To maintain the continuity of solution between the two neighboring zones, the spline interpolation method was used. In this process, the parameter values did not change with

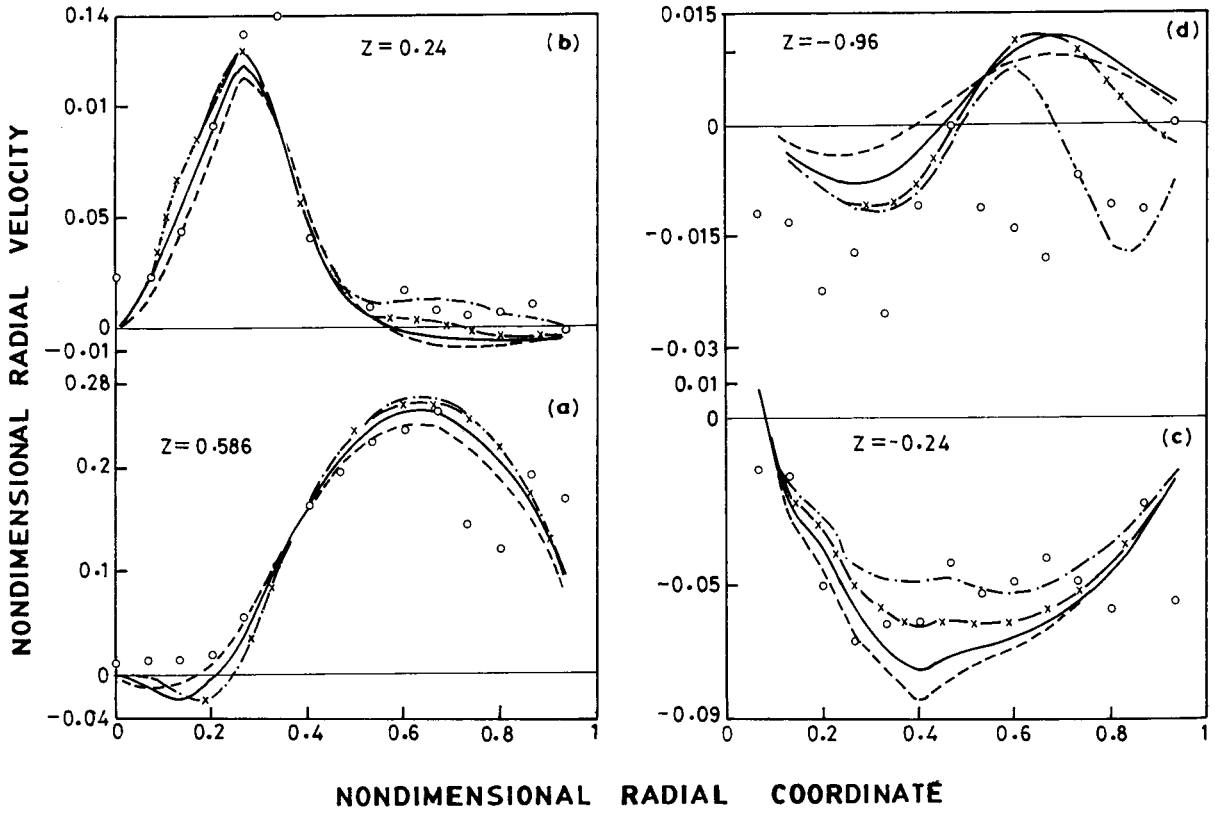

Figure 4. Effects of parameters C_D, C_1, and C_2 on radial velocity. Key: (—) $C_D = 0.09$, $C_1 = 1.44$, $C_2 = 1.92$; (- - -) $C_D = 0.09$, $C_1 = 1.214$, $C_2 = 1.92$; (-·-) $C_D = 0.09$, $C_1 = 1.44$, $C_2 = 1.623$; (-x-x) $C_D = 0.05$, $C_1 = 1.44$, $C_2 = 1.92$; (°°°°°) experimental data.

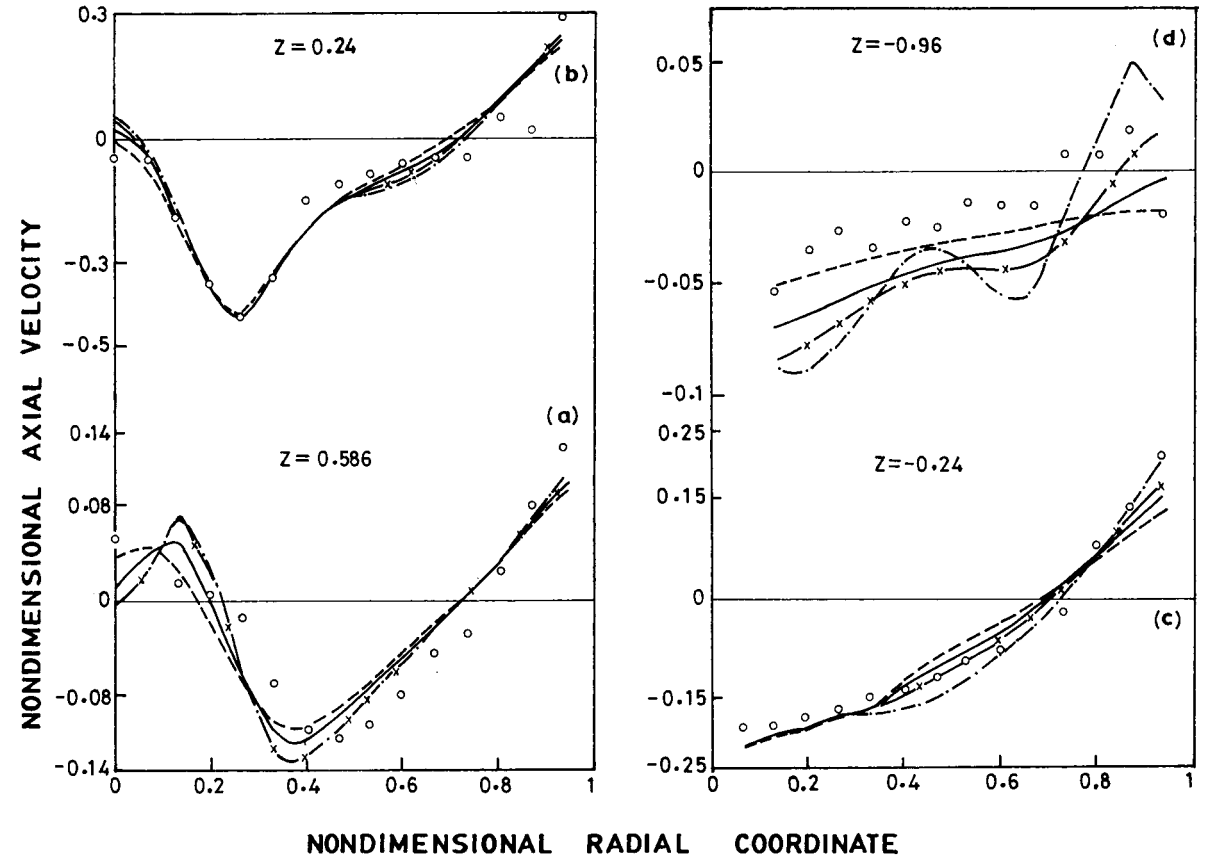

Figure 5. Effects of parameters C_D, C_1, and C_2 on axial velocity. Symbols are the same as in Figure 4.

respect to the angular position. To demonstrate the usefulness of zonal modeling, the predicted flow characteristics were compared with the experimental data and predictions made with the standard set of turbulent parameters. (For the sake of brevity, the predicted results obtained by the zonal modeling will henceforth

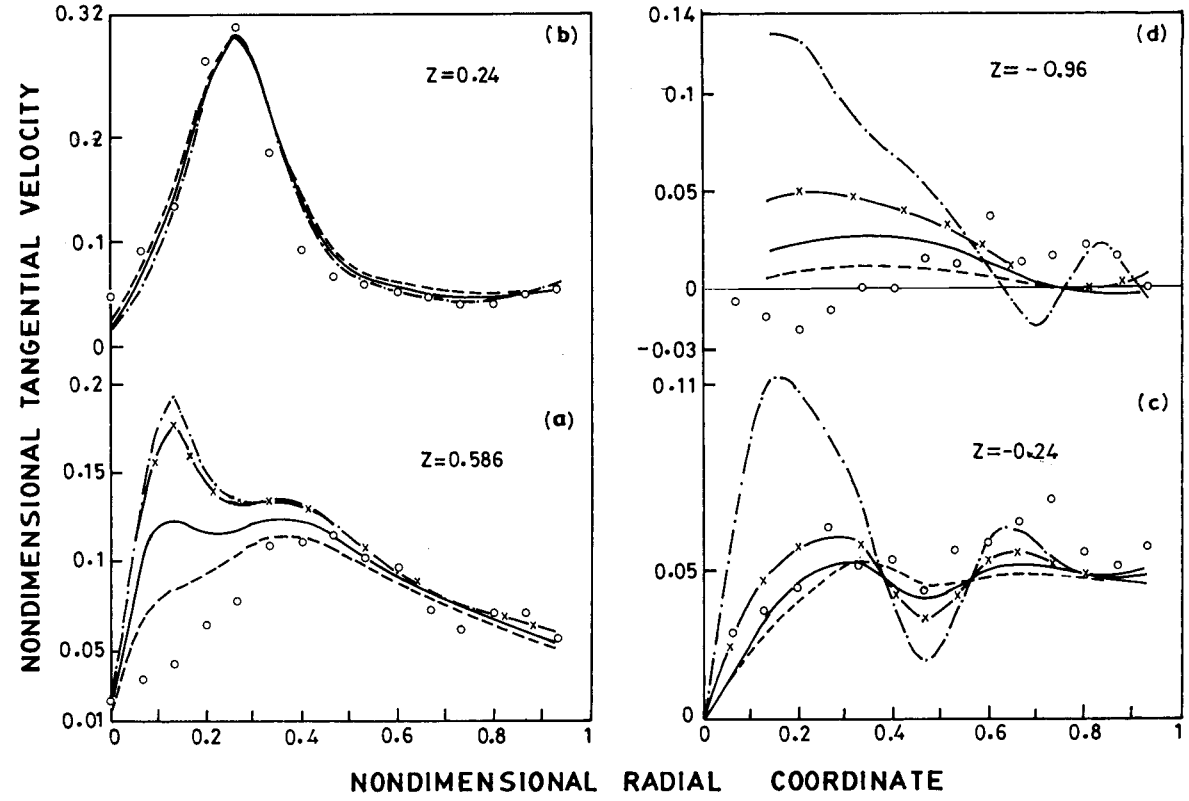

Figure 6. Effects of parameters C_D, C_1, and C_2 on tangential velocity. Symbols are the same as in Figure 4.

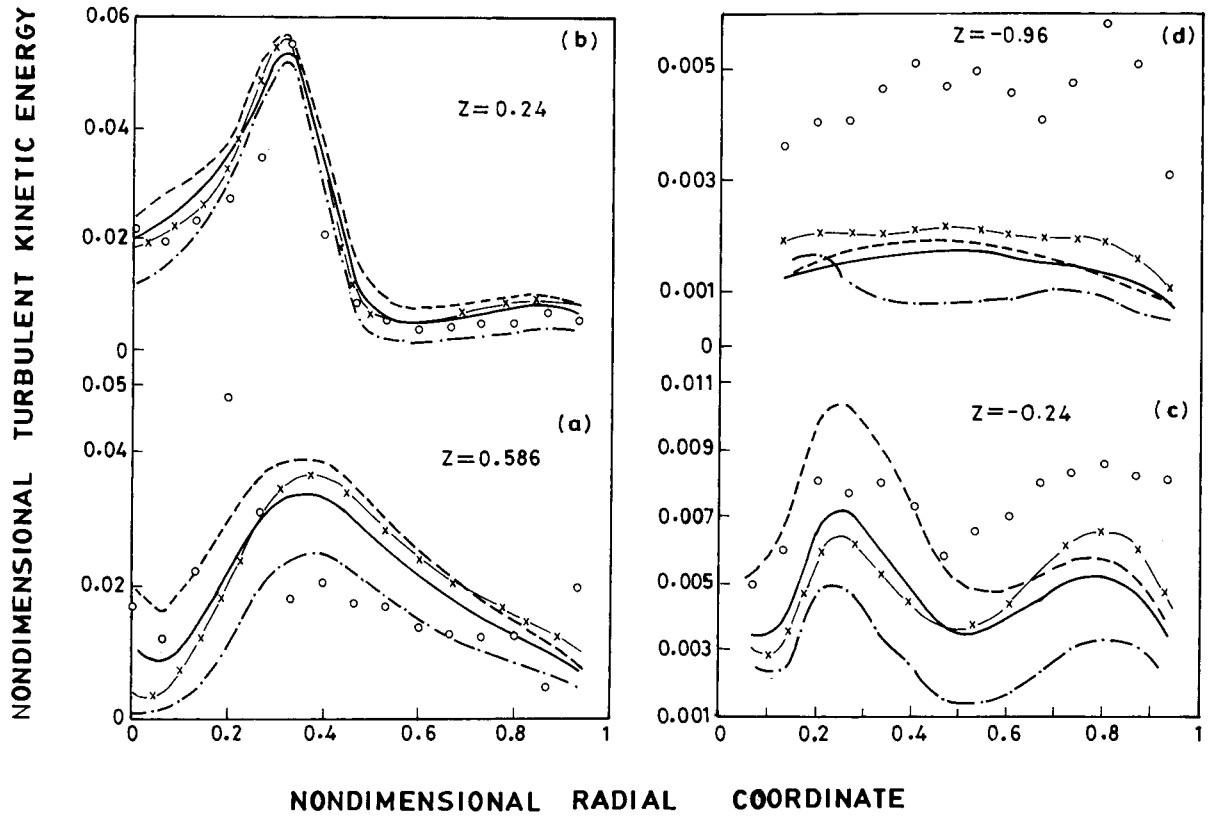

Figure 7. Effects of parameters C_D, C_1, and C_2 on turbulent kinetic energy. Symbols are the same as in Figure 4.

be called *Z-P* and those made by the standard set of turbulent parameters will be named *S-P*.) The turbulent parameter values for zonal modeling are shown in Table 4. The values of these parameters were selected on the basis of their effects on flow characteristics to get a good agreement between predicted and experimental values. Looking at the parameter values, at present, it has not been possible to present a general expression for the variation of parameter values. However, the change in values of C_2 below the impeller is in accordance with the results of Rodi (1993), who modified the values of C_2 for an axisymmetric jet flow

Table 4. Turbulence Model Parameters for Zonal Modeling

	r							
z	0	0.2	0.3	0.5	0.55	0.85	0.97	1.0
				C_D				
0.667	0.25	0.25	0.05	0.050	0.050	0.05	0.09	0.09
0.567	0.25	0.25	0.05	0.050	0.050	0.05	0.09	0.09
0.267	0.09	0.09	0.05	0.050	0.050	0.05	0.09	0.09
0.067	0.09	0.09	0.09	0.090	0.090	0.09	0.09	0.09
−0.133	0.09	0.09	0.09	0.090	0.090	0.09	0.09	0.09
−0.333	0.09	0.09	0.09	0.090	0.090	0.09	0.09	0.09
−0.533	0.09	0.09	0.09	0.090	0.090	0.09	0.09	0.09
−0.733	0.09	0.09	0.09	0.090	0.090	0.09	0.09	0.09
−0.933	0.07	0.07	0.07	0.100	0.100	0.07	0.07	0.07
−1.133	0.05	0.05	0.05	0.125	0.125	0.05	0.05	0.05
−1.333	0.04	0.04	0.04	0.125	0.125	0.04	0.04	0.04
				C_1				
0.667	1.440	1.440	1.440	1.440	1.440	1.440	1.440	1.440
0.567	1.440	1.440	1.440	1.440	1.440	1.440	1.440	1.440
0.267	1.440	1.440	1.400	1.400	1.440	1.440	1.440	1.440
0.067	1.440	1.440	1.440	1.440	1.000	1.000	1.000	1.000
−0.133	1.440	1.440	1.440	1.440	1.000	1.000	1.000	1.000
−0.333	1.440	1.440	1.440	1.440	1.000	1.000	1.000	1.000
−0.533	1.144	1.144	1.144	1.144	1.440	1.440	1.440	1.440
−0.733	1.144	1.144	1.144	1.144	1.440	1.440	1.440	1.440
−0.933	1.144	1.144	1.144	1.144	1.440	1.440	1.440	1.440
−1.133	1.144	1.144	1.144	1.144	1.440	1.440	1.440	1.440
−1.333	1.144	1.144	1.144	1.144	1.440	1.440	1.440	1.440
				C_2				
0.667	1.920	1.920	1.500	1.500	1.500	1.500	1.500	1.500
0.567	1.920	1.920	1.500	1.500	1.500	1.500	1.500	1.500
0.267	1.920	1.920	1.500	1.500	1.500	1.500	1.500	1.500
0.067	1.920	1.920	1.620	1.620	1.620	1.620	1.620	1.620
−0.133	1.920	1.920	1.920	1.920	1.920	2.220	2.220	2.220
−0.333	1.920	1.920	1.920	1.920	1.920	2.220	2.220	2.220
−0.533	2.100	2.100	1.920	1.920	2.200	2.200	2.200	2.200
−0.733	2.300	2.300	1.920	1.920	2.500	2.500	2.500	2.500
−0.933	2.400	2.400	1.920	1.920	2.400	2.400	2.400	2.400
−1.133	2.500	2.500	1.920	1.920	2.600	2.600	2.600	2.600
−1.333	2.600	2.600	1.920	1.920	2.700	2.700	2.700	2.700

in terms of dimensionless jet width, maximum velocity difference, and gradients of maximum velocity. The values of C_2 obtained using this expression is less than the standard value. The impeller stream of the pitched blade turbine can be considered a jet flow and the values used for the present calculation are also less than the standard value, which confirms the observation of Rodi (1993). As evident in Figures 8b and c, the predicted radial velocity profiles with *Z-P* at $z = 0.24$ and $z = 0.36$ were in excellent agreement with the experimental data. The same agreement was not evident between the result predicted by *S-P* and the experimental data. In particular, the peak values were not predicted accurately by *S-P*. Furthermore, in the range $0.6 < r < 0.8$, the profiles predicted by *Z-P* merged with the experimental data, which was not true for *S-P*. Similar behavior was also observed for turbulent kinetic energy (Figures 11b and c) for $r > 0.4$. For $r < 0.4$, both *S-P* and *Z-P* overpredicted the turbulent kinetic energy. However, *S-P* and *Z-P* yielded almost the same result for the axial and tangential velocities (Figures 9b and c and Figures 10b and c) at the said locations. At $z = 0.586$, the radial velocity profiles predicted by *S-P* and *Z-P* were almost (Figure 8a) the same and in good agreement with the experimental data for $r < 0.6$. The axial velocity predicted by *Z-P* at this location was in better agreement with the experimental data than that predicted by *S-P* (Figure 9a). The same comparison could also be made for the prediction of tangential velocity (Figure 10a) and turbulent kinetic energy (Figure 11a). These results clearly indicate that the zonal modeling improved the predictions below the impeller. From the literature review, it was seen that the main region of disagreement between the experimental and the predicted values was above the impeller. Therefore, a detailed comparison between the predictions of *Z-P* and the experimental data above the impeller was needed. At $z = -0.24$, the radial velocity profile predicted by *Z-P* was in better agreement with the experimental data than the profile predicted by S-P (Figure 8d). An excellent agreement between the experimental data and *Z-P* prediction was also observed for axial velocity profile (Figure 9d) at this location. A good agreement between the tangential velocity predicted by S-P and the experimental data was observed for $r < 0.5$ (Figure 10d). The profile predicted by *Z-P* was slightly lower than the *S-P* prediction (Figure 10d). For $r \geq 0.5$, both the predicted profiles were almost the same and lower than the experimental data (Figure 10d). A similar observation was also made for the velocity profiles at $z = -0.48$ (Figures 8e, 9e, and 10e). The values of k at $z = -0.24$ (Figure 11d) determined by *Z-P* were overpredicted for $r \leq 0.6$ and in good agreement with experimental data for $r > 0.6$. In contrast, *S-P* underpredicted the values of k for all r. It may be observed from Figure 11e that

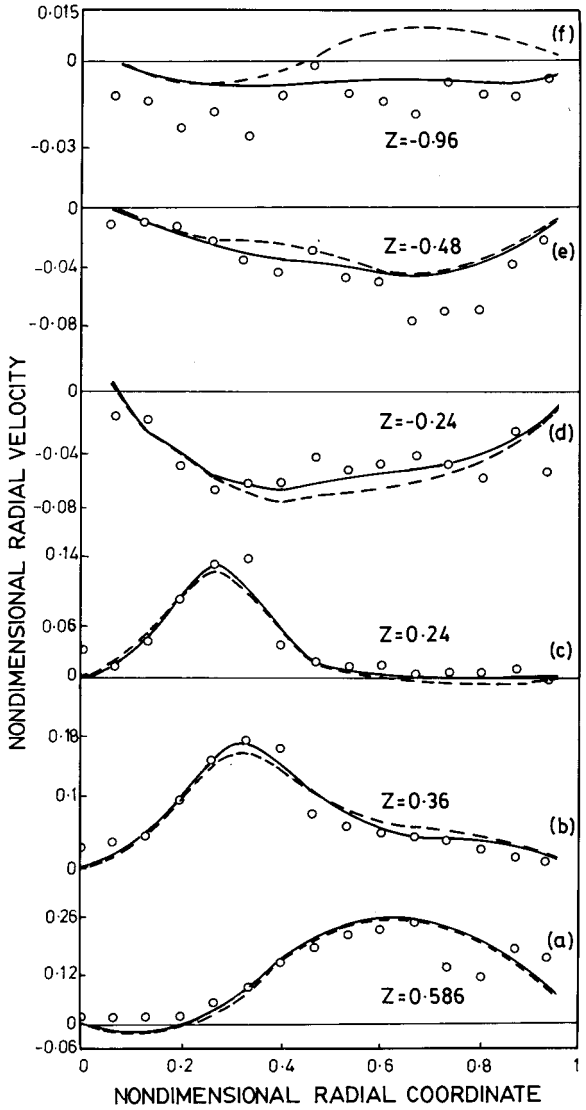

Figure 8. Comparison of predicted values of radial velocity with experimental value. Key: (—) *Z-P*; (- - -) *S-P*, (°°°°°) experimental data.

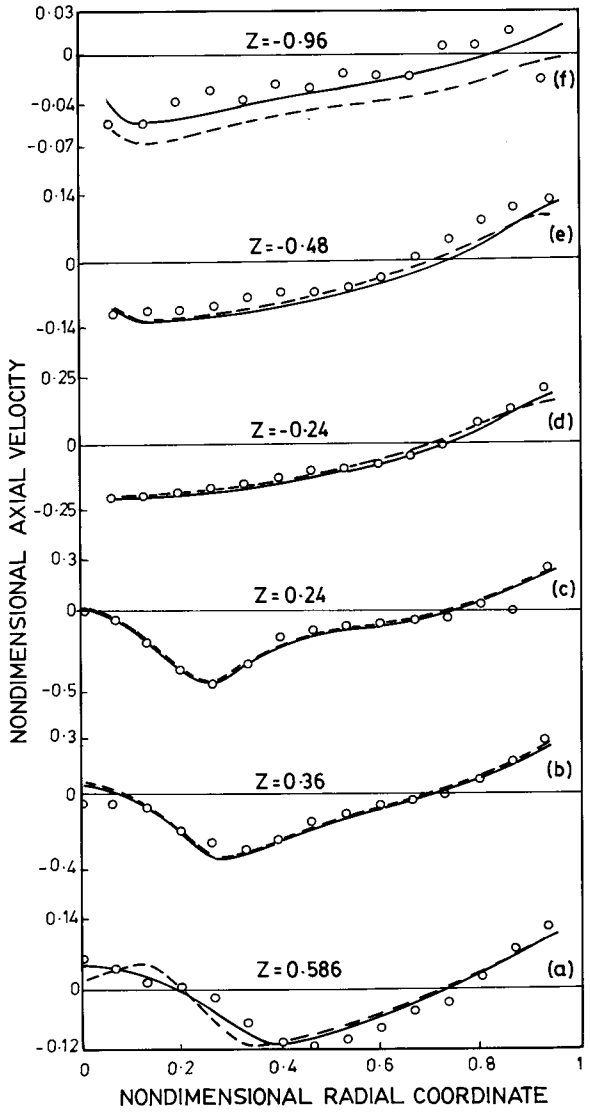

Figure 9. Comparison of predicted values of axial velocity with experimental value. Symbols are the same as in Figure 8.

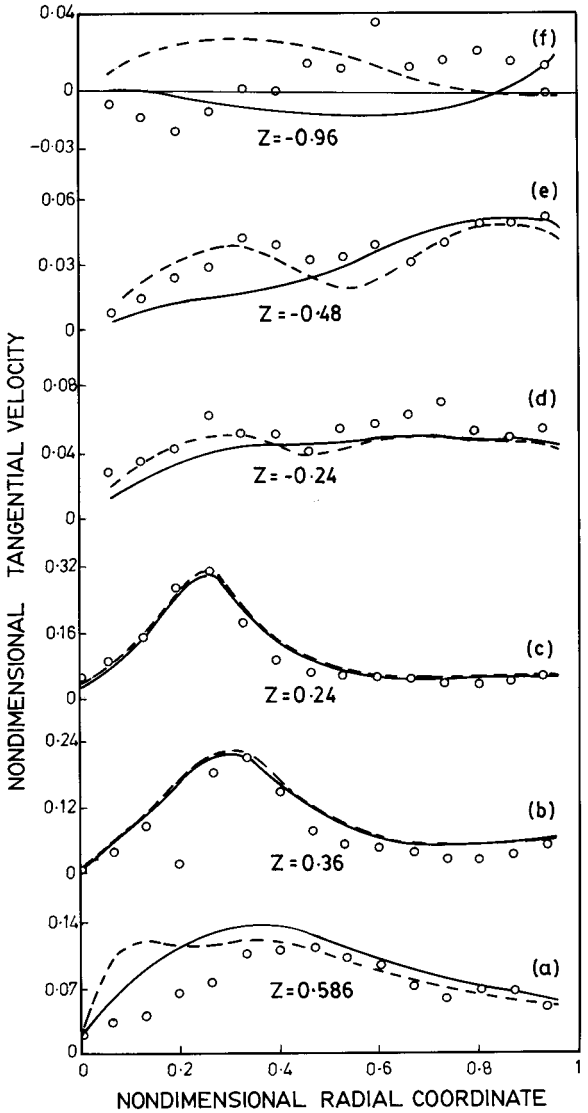

Figure 10. Comparison of predicted values of tangential velocity with experimental value. Symbols are the same as in Figure 8.

the k profile predicted by *Z-P* is in very good agreement with the experimental data for $r < 0.65$. The *S-P* predictions of k were very small compared with the experimental data (Figure 11e). At $z = -0.96$, the radial and axial velocity predicted by *Z-P* were seen closer to the experimental data (Figure 8f and 9f). The radial velocity profile (Figure 8f) at this position predicted by *S-P* behaved in the opposite manner compared with the experimental data. The tangential velocity profile predicted by *S-P* also behaved in exactly the opposite manner compared with the experimental data (Figure 10f). However, *Z-P* predicted the tangential velocity that was comparable to the experimental data (Figure 10f). *S-P* predicted a very low turbulent kinetic energy (Figures 11e and f), whereas *Z-P* predicted turbulent kinetic energy that agreed well with the experimental value except within the region $r > 0.65$ (Figures 11e and f). The near wall discrepancy might be due to the wall boundary condition. From these results, it is clear that the introduction of zonal modeling improves the predicted flow characteristic in the entire vessel. Furthermore, by tuning the model parameters and employing zonal modeling, the efficiency of the turbulent k-ϵ model could be enhanced for the simulation of flow in stirred vessels.

It is well known that there is no direct method for the experimental measurement of turbulent energy dissipation rate. However, from time to time, attempts have been made by various researchers to calculate ϵ from fluctuating velocity by using some correlation. In the literature, various correlations have been proposed. The formula proposed by Wu and Patterson (1989) seems to be more appropriate and has been used in the present calculation. As seen in Figure 12, below the impeller, the energy dissipation rate predicted by *Z-P* and *S-P* is almost the same except very close to the vessel bottom. The predicted values are in good agreement with experimental data for $r \geq 0.4$ (Figures 12a and b). Close to the vessel bottom, the predicted values obtained by *Z-P* are in better agreement with experimental values than the values predicted by *S-P* (Figure 12c). Above the impeller also, the predicted values behave in similar manner when they are close to the impeller (Figure 12d). As one moves away from the impeller, a wide difference between the predicted values and the experimental data can be observed, irrespective of the models (Figures 12e and f). However, the values predicted by *Z-P* are better than those predicted by *S-P*.

The variation in flow characteristics due to zonal modeling may be explained in terms of eddy viscosity.

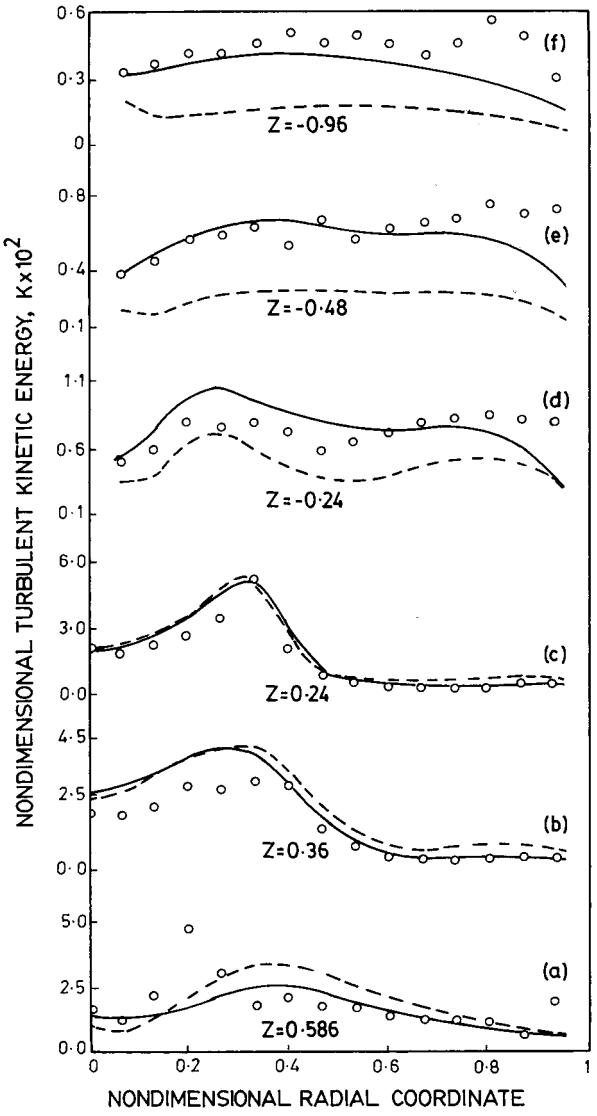

Figure 11. Comparison of predicted values of turbulent kinetic energy with experimental value. Symbols are the same as in Figure 8.

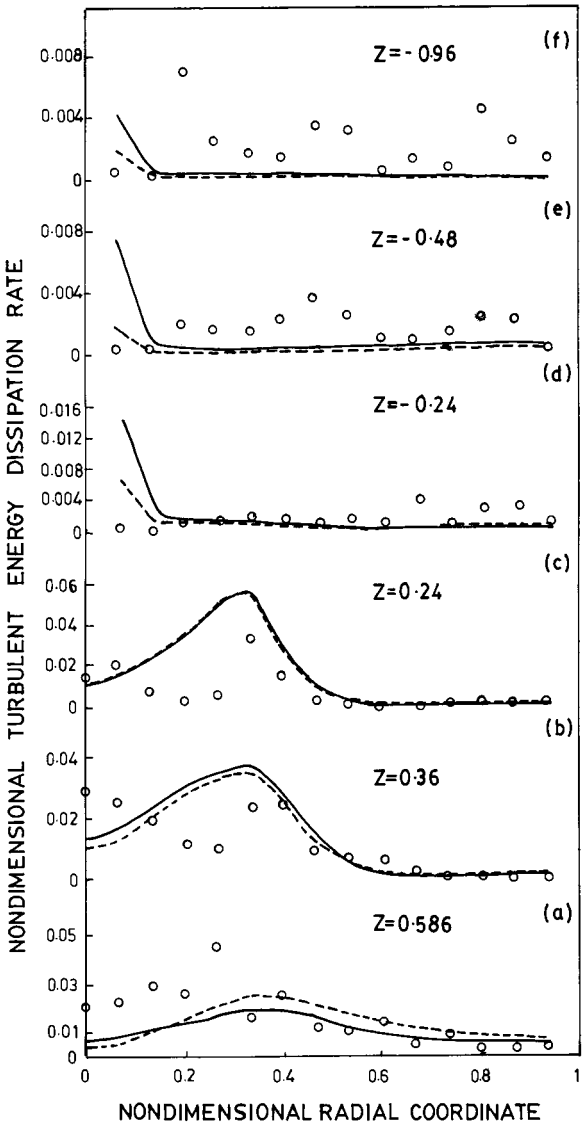

Figure 12. Comparison of predicted values of turbulent energy dissipation rate with experimental value. Symbols are the same as in Figure 8.

The parameter C_2 appears in the sink term (Table 3); that is, the term by which the dissipated energy is converted to heat. As C_2 decreases, it causes a decrease in energy dissipation rate. As a result, there is a decrease in the turbulent kinetic energy. The overall effect of the changes in ϵ and k causes a decrease in eddy viscosity and increase in velocity gradients. An opposite behavior is observed with the decrease in C_1 because it is the coefficient of generation term. It is also well known that lowering the value of C_D decreases the eddy viscosity. These observations may be seen in Figures 5−8.

Conclusion

The parametric effect study revealed the difficulty of obtaining a single set of parameters that could predict all the flow characteristics close to the experimental data. So the concept of zonal modeling was introduced. The agreement between the experimental and the predicted flow characteristics with zonal modeling was very good for most of the flow characteristics; namely, three components of the velocity and the turbulent kinetic energy except ϵ. The agreement between experimental and predicted ϵ with zonal modeling was very good close to the bottom of the vessel. Although zonal modeling improved the predictions above the impeller, agreement with experimental ϵ was not good. However, the predictions of flow characteristics in the entire tank can be improved further by tuning the turbulent model parameters in different zones. Therefore the k-ϵ model can successfully be used for the simulation of a stirred tank with zonal modeling. It may be interesting to note that the set of parameters chosen for the present study holds good for other axial flow impellers, such as a curved pitched blade turbine, a multibladed pitched turbine, a propeller, and a modified propeller.

Acknowledgment

The authors are grateful to the Department of Biotechnology, Government of India, for the award of project no. BT/12/11/PRO 485/97.

Nomenclature

C_1 = empirical constant in the dissipation equation
C_2 = empirical constant in the dissipation equation

C_D = empirical constant relating eddy viscosity, k and ϵ
CFD = computational fluid dynamics
CMV = comparison of mean velocities
CPU = central processing unit
CTP = comparison of turbulent parameters
D = impeller diameter, m
H = height of liquid in the tank, m
H_c = clearance between impeller center and vessel bottom, m
k = dimensionless turbulent kinetic energy,
L_{res} = resultant length scale, m
P_p = power calculated from power number, watts
P_e = power calculated from experiment, watts
p = dimensionless pressure
r = nondimensional radial coordinate
r_b = nondimensional distance between vessel center and baffle edge
r_s = dimensionless radius of shaft
RMS = root mean square
S-P = predicted results obtained with standard parameters
S_ϕ = source term for the generalized variable ϕ
T = vessel diameter, m
U_{tip} = impeller tip velocity, m/s
u = dimensionless mean radial velocity
v = dimensionless mean axial velocity
w = dimensionless mean tangential velocity
w_s = dimensionless tangential velocity at shaft surface
Z-P = predicted results obtained by zonal modeling
z = nondimensional axial coordinate

Greek Symbols

α_v = relaxation parameter for velocities
α_p = relaxation parameter for pressure
Γ_{eff} = effective viscosity for the variable ϕ
γ = Von Karman constant
ϵ = dimensionless turbulent energy dissipation rate
θ = tangential coordinate
μ = dimensionless parameter
$\bar{\mu}$ = viscosity, Pa·s
μ_t = nondimensional eddy viscosity
ρ = density of water, kg/m^3
σ_k = Prandtl number for turbulent kinetic energy
σ_ϵ = Prandtl number for turbulent kinetic energy dissipation rate
ϕ = generalized notation for transport variable

Literature Cited

Abujelala, M. T.; Lilley, D. G. Limitations and empirical extensions of the k-ϵ model as applied to turbulent confined swirling flows. *Chem. Eng. Commun.* **1984**, *31*, 223−236.

Armenante, P. M.; Chou, C. C. Velocity profiles in a baffled vessel with single or double pitched blade turbines. *AIChE J.* **1996**, *42*, 42−54.

Bakker, A.; Van den Akker, H. E. A. Single-phase flow in stirred reactors. *Trans Inst. Chem. Eng.* **1994**, *72*, 583−593.

Brucato, A.; Ciofalo, M.; Grisafi, F.; Micale, G. Complete numerical solution of flow fields in baffled stirred vessels: The inner-outer approach. *Inst. Chem. Eng. Symp. Series* **1994**, *136*, 155−162.

Desouza, A.; Pike, R. W. Fluid dynamics and flow patterns in stirred tanks with a turbine impeller. *Can. J. Chem. Eng.* **1972**, *50*, 15−23.

Drbohlav, J.; Fort, I.; Maca, K.; Placek, J. Turbulent characteristics of discharge flow from turbine impeller. *Coll. Czech. Chem. Commun.* **1978**, *43*, 3148−3162.

Ferziger, J. H.; Kline, S. J.; Avva, R. K.; Bordalo, S. N.; Tzuoo, K. L. Zonal modelling of turbulent flows - Philosophy and accomplishments: Near wall turbulence. *Zoran Zaric Memorial Conference*, Kline, S. J., Afgan, N. H., Eds.; 1988; pp 801−817.

Fokema, M. D.; Kresta, S. M.; Wood, P. E. Importance of using the correct impeller boundary conditions for CFD simulations of stirred tanks. *Can. J. Chem. Eng.* **1994**, *72*, 177−183.

Fort, I. Studies on mixing XIX - Pumping capacity of propeller mixer. *Coll. Czech. Chem. Commun.* **1967**, *32*, 3663−3678.

Fort, I. Flow and turbulence in vessels with axial impeller. *Mixing Theory And Practice, Vol. III*; Uhl, V. W., Gray, J. B., Eds.; Academic: New York, 1986.

Fort, I.; Neugebauer, R.; Pastyrikova, M. Studies on Mixing XXIX - Spatial distribution of mechanical energy dissipated by axial impeller in a system with radial baffles. *Coll. Czech. Chem. Commun.* **1971**, *36*, 1769−1793.

Fort, I.; Vonzy, M.; Forstova, B. Distribution of turbulence characteristics in agitated systems with axial high speed impeller and baffles. *7th European Conference on Mixing*, 1991; pp 33−41.

Harris, C. K.; Roekaerts, D.; Rosendal, F. J. J. Computational fluid dynamics for chemical reactor engineering. *Chem. Eng. Sci.* **1996**, *51*, 1569−1594.

Harvey, P. S.; Greaves, M. G. Turbulent flow in an agitated vessel part-I: A predictive model. *Trans. Inst. Chem. Eng.* **1982**, *60*, 195−200.

Harvey, P. S.; Greaves, M. G. Turbulent flow in an agitated vessel part-II: Numerical solution and model predictions. *Trans. Inst. Chem. Eng.* 1982, *60*, 201−210.

Hockey, R. M.; Nouri, J. M. Turbulent flow in a baffled vessel stirred by a 60° pitched blade impeller. *Chem. Eng. Sci.* **1996**, *51*, 4405−4421.

Hwang, C. C.; Zhu, G.; Massoudi, M.; Ekmann, J. M. A comparison of the linear and non linear k-ϵ turbulence models in combusters. *ASME J. Fluid Eng.* **1993**, *115*, 93−102.

Jaworski, Z.; Fort, I. Energy dissipation rate in a baffled vessel with pitched blade turbine impeller. *Coll. Czech. Chem. Commun.* **1991**, *56*, 1856−1867.

Jaworski, Z.; Nienow, A. W.; Koutsakos, E.; Dyster, K.; Bujalski, W. An LDA study of the turbulent flow in a baffled vessel agitated by a pitched blade turbine. *Chem. Eng. Res. Des.* **1991**, *69*, 313−320.

Kresta, S. M.; Wood, P. E. The Mean flow field produced by a 45 degree pitched blade turbine: Changes in the circulation pattern due to off bottom clearance. *Can. J. Chem. Eng.* **1993a**, *71*, 42−53.

Kresta, S. M.; Wood, P. E. The flow field produced by a Pitched blade turbine: Characterization of the turbulence and estimation of the dissipation rate. *Chem. Eng. Sci.* **1993b**, *48*, 1761−1774.

Launder, B. E.; Spalding, D. B. The numerical computation of turbulent flows. *Comput. Methods Appl. Mech. Eng.* **1974**, *3*, 269−289.

Middleton, J. C.; Pierce, F.; Lynch, P. M. Computations of flow fields and complex reaction yield in turbulent stirred reactors and comparison with experimental data. *Chem. Eng. Res. Des.* **1986**, *64*, 18−22.

Patankar, S. V. *Numerical Heat Transfer and Fluid Flow*; Hemisphere: New York, 1980.

Patel, V. C.; Rodi, W.; Scheuerer, G. Turbulence models for near wall and low Reynolds number flows: A review. *AIAA J.* **1984**, *23*, 1308−1319.

Peric, M.; Kessler, R.; Schellerer, G. Comparison of finite volume numerical methods with staggered and non-staggered grids. *Rept. No. 163/T/87, Lehrst. f. Stromungsmechanik*, Univ. Erlange, Nbg, 1987.

Pericleous, K. A.; Patel, M. K. The modeling of tangential and axial agitators in chemical reactors. *PCH* **1987**, *8*, 105−123.

Placek, J.; Fort, I.; Strek, F.; Jaworski, Z.; Karcz, Z. Velocity field at the wall of fully baffled vessel with turbine impeller. *Proceedings of the 5th Congress CHISA*, Prague, 1978.

Platzer, B. A contribution to the evaluation of turbulent flow in baffled tanks with radial outflow impellers. *Chem. Technik.* **1981**, *33*, 16−19.

Platzer, B.; Noll, G. An analytical solution for the flow in baffled vessel with radial outflow impellers. *Chem. Technik.* **1981**, *33*, 648−655.

Ranade, V. V.; Joshi, J. B. Flow generated by pitched blade turbines I: Measurements using laser Doppler anemometer. *Chem. Eng. Commun.* **1989a**, *81*, 197−224.

Ranade, V. V.; Joshi, J. B.; Marathe, A. G. Flow generated by pitched blade turbines II: Simulation using k-ϵ model. *Chem. Eng. Commun.* **1989b**, *81*, 225−248.

Ranade, V. V.; Bourne, J. R.; Joshi, J. B. Fluid mechanics and blending in agitated tanks. *Chem. Eng. Sci.* **1991**, *46*, 1883−1893.

Ranade, V. V.; Mishra, V. P.; Saraph, V. S.; Deshpande, G. B.; Joshi, J. B. Comparison of the axial flow impellers using laser Doppler anemometer. *Ind. Eng. Chem. Res.* **1992**, *31*, 2370−2379.

Ranade, V. V.; Dommeti, S. M. S. Computational snapshot of flow generated by axial impellers in baffled stirred vessels. *Trans. Inst. Chem. Eng.* **1996**, *74*, 476−484.

Rodi, W. Turbulence models and their application in hydraulics: Monograph. A. A. Balkema: Netherlands, 1993.

Sahu, A. K.; Joshi, J. B. Simulation of flow in stirred vessels with axial flow impellers: Effects of various numerical schemes and turbulence model parameters. *Ind. Eng. Chem. Res.* **1995**, *34*, 626−639.

Tatterson, G. B.; Yuan, H. S.; Brodkey, R. S. Stereoscopic visualization of the flows for pitched blade turbines. *Chem. Eng. Sci.* **1980**, *35*, 1369−1375.

Van doormal, J. P.; Raithby, G. D. Enhancements of the SIMPLE method for predicting incompressible fluid flows. *Num. Heat Transfer* **1984**, *7*, 147−163.

Wu, H.; Patterson, G. K. Laser Doppler measurements of turbulent flow parameters in a stirred mixer. *Chem. Eng. Sci.* **1989**, *44*, 2207−2221.

Xu, Y.; Mcgrath, G. CFD predictions in stirred tank flows. *Trans. Inst. Chem. Eng.* **1996**, *74*, 471- 475.

Received for review May 6, 1997
Revised manuscript received November 3, 1997
Accepted November 5, 1997

IE970321S